Wuhan University
Journal of Natural Sciences

2026, Vol.31 No.2, 121-132

Article ID 1007-1202(2026)02-0121-12 DOI https://doi.org/10.1051/wujns/2026312121

Cite this article: QIN Tao, TANG Hongliang, ZHENG Liangqiu, *et al*. UV-Cu/Mn-Zeolite Heterogeneous Fenton Method for Degradation of Sulfamethoxazole[J]. *Wuhan Univ J of Nat Sci*, 2026, 31(2): 121-132.

# UV-Cu/Mn-Zeolite Heterogeneous Fenton Method for Degradation of Sulfamethoxazole

□ **QIN Tao[1], TANG Hongliang[1], ZHENG Liangqiu[1], DING Sicheng[2], LI Jianbing[3], ZENG Xiaolan[1†]**

1. College of Environment and Ecology, Chongqing University, Chongqing 400045, China;
2. Department of Chemistry , Duke University, Durham, North Carolina 27708, USA;
3. School of Engineering, University of Northern British Columbia (UNBC), Prince George V2N4Z9, British Columbia, Canada

**Abstract:** Sulfamethoxazole (SMX) and other antibiotics pose significant risks to humans and the environment even at trace concentrations, whereas conventional physicochemical and biological degradation methods are often ineffective. This study employed an integrated strategy combining photocatalysis with heterogeneous Fenton technology for SMX removal, and compared the removal efficiency of the UV-$H_2O_2$ and the UV-zeolite-supported Cu/Mn bimetallic heterogeneous Fenton method. The results demonstrate that the catalytic activity is primarily influenced by the calcination temperature, followed by the calcination time and the Cu/Mn molar ratio in the impregnation solution. The optimal catalyst is prepared with a Cu/Mn molar ratio of 2∶1 and calcined at 300 ℃ for 3 h. In the catalyst, copper and manganese exist primarily as CuO, $Cu_2O$, Cu/Mn oxides, and $MnO_2$/$Mn_3O_4$. At pH=7.2 and an initial SMX concentration of 20 mg/L, the optimized UV-Cu /Mn-zeolite heterogeneous Fenton system with 0.15 g/L catalyst and 7.5 mmol/L $H_2O_2$ achieved a 77.3% SMX removal rate. This represents a 15.1% improvement over the conventional UV-$H_2O_2$ process, and the degradation follows pseudo-first-order kinetics. Metal leaching remained below 0.5 mg/L after 90-min reaction, and the catalyst lost less than 5% of its initial activity after four reuse cycles.

**Key words:** Cu/Mn-zeolite catalyst; UV-heterogeneous Fenton system; sulfamethoxazole (SMX); optimal preparation conditions; reaction condition; catalyst stability

**CLC number**: X703

## 0 Introduction

Sulfonamide antibiotics have become one of the most prevalent classes of antibiotics in global aquatic environments due to their extensive use, high chemical stability, and hydrophilicity[1]. Among them, sulfamethoxazole (SMX) is one of the most frequently detected sulfonamides. Even at low concentrations, SMX can induce pathogen resistance, disrupt normal biological systems functions, and pose a significant threat to ecosystems and human health.

Currently, various technologies including physical adsorption, membrane separation, biological degradation, and oxidative degradation are employed for SMX removal from water bodies[2-3]. Physical techniques such as activated carbon adsorption and nanofiltration merely separate SMX rather than completely degrade the pollut-

**Received date:** 2025-06-26 

**Foundation item:** Supported by the Research Project of Power China Chengdu Engineering Corporation Limited (P45220) and the Large-Scale Instruments & Equipment Open-End Fund of Chongqing University (202503150095, 202303150061, 202303150125)

**Biography:** QIN Tao, male, Master candidate, research direction: wastewater treatment. E-mail: 1421483579@qq.com

† Corresponding author. E-mail: wendyzeng@cqu.edu.cn

ant[4]. Biological treatments like activated sludge show low removal efficiency due to the poor biodegradability of SMX.

In the realm of oxidative technologies, advanced oxidation processes (AOPs) have been widely employed for the degradation of complex organic pollutants due to their high efficiency and environmental friendliness. As a representative AOP, the classic Fenton oxidation has been successfully utilized by Chi *et al*[5] to remove antibiotic micropollutants such as sulphapyridine (SPY), sulfamethazine (SMZ), and SMX from biogas slurry. However, this method is highly sensitive to pH variations. Zhao *et al*[6] investigated the impact of pH on SMX wastewater treatment using classic Fenton oxidation. Their results revealed that the maximun COD removal efficiency was achieved at pH=3, with the performance diminishing at either more acidic or more alkaline pH values. Furthermore, classical Fenton processes are prone to side reactions, which significantly compromise reagent utilization.

Iron-based heterogeneous Fenton systems address these limitations by stabilizing iron species within solid catalysts, enabling effective $H_2O_2$ activation to generate ·OH over a wider pH range[7] and increasing the reusability of catalysts. Nevertheless, relatively low reaction rates of the catalysts (due to limited contact area with $H_2O_2$ and pollutants) and the formation of iron sludge deposition on the catalyst surface under neutral pH conditions[8] remain problematic. These issues can be mitigated by incorporating UV irradiation to construct UV-heterogeneous Fenton systems[9]. Studies show that transition metals like Cu and Mn with abundant oxygen vacancies and tunable redox properties can serve as effective substitutes for Fe to catalyze $H_2O_2$ for ·OH generation. These alternative transition metals are also advantageous in reducing metal sludge formation under near-neutral pH[10-11]. To enhance catalyst reusability[7], activity, and cost-effectiveness, bimetallic or multimetallic systems have become a key research focus[12]. Among these, Cu-Mn composite catalysts prepared by co-precipitation exhibit superior catalytic activity[13-15].

The structural properties of the solid-phase catalyst support also play a pivotal role in determining system performance. Zeolites, a common support for metal catalysts, can significantly increase the surface area and number of active sites[16], which collectively enhance the catalytic efficiency by improving metal dispersion and interfacial reaction kinetics.

In our previous study on heterogeneous Fenton degradation of SMX by single-metal-loaded UV-zeolite, the research group found that the optimal external UV radiation range for SMX removal was 200-280 nm. Additionally, the catalytic activity decreased in the following order: Cu-loaded catalyst > Mn-loaded catalyst > Co-loaded catalyst[17].

Based on these findings, the present study proposes a novel UV-zeolite-supported Cu/Mn bimetallic heterogeneous Fenton technology for the efficient degradation of SMX under near-neutral initial pH conditions, while enhancing catalyst activity and reusability. An orthogonal experimental design was employed to optimize the catalyst preparation parameters, with three levels for each factors: calcination temperature, calcination time, and Cu/Mn molar ratio in the impregnation solution. Subsequently, the zeolite-supported Cu/Mn bimetallic catalyst was synthesized via a co-precipitation method. Based on the structural and compositional characterization of the optimal catalyst, the single-variable method was used to investigate the optimal dosages of catalyst and $H_2O_2$ for the UV-zeolite-supported Cu/Mn bimetallic heterogeneous Fenton oxidation of SMX under different reaction conditions. The performance of this system was compared with that of the conventional UV-$H_2O_2$ oxidation process to evaluate the feasibility of applying the UV-zeolite-supported Cu/Mn bimetallic heterogeneous Fenton system for SMX degradation.

# 1 Experimental

## 1.1 Reagents and Instruments

All reagents were used as received without further purification unless otherwise noted.

Reagents: SMX, p-dimethylaminobenzaldehyde (PDAB), 30% $H_2O_2$, anhydrous ethanol, sodium hydroxide, methanol, concentrated sulfuric acid, concentrated nitric acid, manganese dioxide, anhydrous copper sulfate, and manganese sulfate (all of analytical grade); and synthetic zeolite ($Na_2{\cdot}Al_2O_3{\cdot}x SiO_2{\cdot}y H_2O$, 40-60 mesh, of chemical purity).

Preparation of SMX solution: SMX was dissolved in methanol to prepare a stock solution with a concentration of 2 g/L, which was then diluted with deionized water to obtain a working solution of 20 mg/L. The initial pH of the solution was adjusted to 7.2.

The PDAB chromogenic reagent was prepared by dissolving 1 g of PDAB in 50 mL of anhydrous ethanol

and adding 3.2 mL of concentrated nitric acid to adjust the pH of the solution.

Instruments: UV lamp (UV-8W, Guanya Optoelectronic Technology Co., Ltd.), magnetic stirrer (HJ-4A, Changzhou Guoyu Instrument Manufacturing Co., Ltd.), UV-Vis spectrophotometer (T6 New Century, Beijing Purkinje General Instrument Co., Ltd.), scanning electron microscope (SEM, VEGA 3 LMH, Tescan), Fourier transform infrared (FTIR) spectrometer (Nicolet iS5, Thermo Fisher Scientific), X-ray diffractometer (XRD, Rigaku D/MAX 2500, Rigaku Corporation, Japan), muffle furnace (SX-4-10 type box-type resistance furnace control unit, Tianjin Test Instruments Co., Ltd.), and analytical balance (FA2004B, Shanghai Precision Scientific Instrument Co., Ltd.).

## 1.2 Setup

The research employed a self-made reaction device shown in Fig. 1. The 8W UV lamp with a wavelength of 254 nm was preheated for 15 min. All experiments were conducted at (25 ± 2) °C with 100 mL of unadjusted pH solution stirred at 200 r/min.

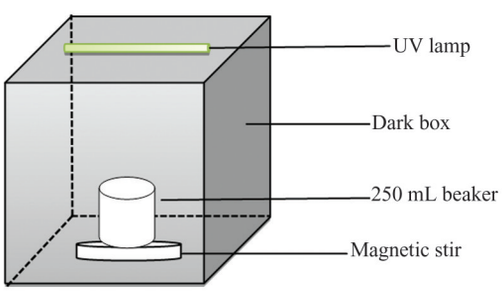


**Fig. 1 Simple sketch of homemade reaction device**

## 1.3 Experimental Method

1.3.1 Catalyst preparation and optimization

Three influencing factors, namely calcination time, calcination temperature, and Cu/Mn molar ratio in the impregnation solution, were each set at three levels, with an additional blank column. The calcination time was set at three levels ($i$=1, 2, 3): 3, 4, and 5 h; the calcination temperature was set at 300, 400, and 500 ℃; and the Cu/Mn molar ratio was set at 2∶1, 2∶2, and 2∶0.5, respectively. Nine catalysts were prepared via an $L_9(4^3)$ orthogonal array design according to the following steps:

1) Pretreatment: Zeolite was washed with deionized water until the eluate became clear, and then dried to constant weight at 80 ℃.

2) Impregnation and aging: The pretreated zeolite was added into the impregnation solution at a concentration of 100 g/L, with the $Cu^{2+}$ concentration fixed at 0.16 mol/L and different Cu/Mn molar ratios controlled. The mixture was stirred at 200 r/min for 12 h, titrated to pH 8 using 0.1 mol/L NaOH solution, and aged for 4 h. After filtration, the solid product was washed with ultrapure water and dried to constant weight at 100 ℃.

3) Calcination: The obtained solid was calcined in a crucible using a muffle furnace, with precise control over calcination time and temperature.

The optimal catalyst preparation conditions were quantitatively evaluated based on the SMX removal efficiency, followed by comprehensive characterization of the best-performing catalyst.

1.3.2 SMX degradation

Each prepared catalyst was tested in standard reactions containing 20 mg/L SMX and 7.5 mmol/L $H_2O_2$ for 90 min. Every 15 min, 1 mL of sample was filtered through a 0.45 μm filter membrane, and 0.05 mL of ethanol was added to the filtrate for quenching. The SMX removal efficiency of these catalysts was quantitatively evaluated using a spectrophotometer. To investigate the individual effects of catalyst dosage and $H_2O_2$ dosage on SMX degradation, experiments were carried out by maintaining one variable constant while varying the other. Under optimal conditions (20 mg/L SMX, 0.15 g/L catalyst, 7.5 mmol/L $H_2O_2$), samples were taken every 15 min to compare the SMX degradation efficiency of the UV-$H_2O_2$ oxidation process and the UV-Cu/Mn-zeolite heterogeneous Fenton oxidation process. The kinetics were fitted using the Langmuir-Hinshelwood (L-H) model, as shown in Equations (1) and (2).

$$r = -\frac{\mathrm{d}C}{\mathrm{d}t} = kC, \tag{1}$$

$$\ln\left(\frac{C_0}{C}\right) = kt, \tag{2}$$

where $C$ is the contaminant concentration (mg/L); $C_0$ is the initial contaminant concentration (mg/L); $k$ is the apparent reaction rate constant ($min^{-1}$); $r$ is the reaction rate ($mg \cdot L^{-1}/min$); and $t$ is the reaction time (min).

1.3.3 Catalyst stability tests

The stability of the catalyst prepared under optimal conditions was explored through the following tests. Experiments were conducted with 20 mg/L SMX, 7.5 mmol/L $H_2O_2$, and a catalyst dosage of 0.15 g/L. After predefined reaction intervals, 1 mL of sample was taken, filtered through a 0.45 μm filter membrane, and quenched by adding 0.05 mL of ethanol. Quantitative analysis was performed using a spectrophotometer.

1) Samples were collected at 30-min intervals to quantitatively determine the dissolution concentrations of Cu and Mn via atomic absorption spectroscopy, thereby evaluating the structural stability of the catalyst during degradation.

2) The experiment was repeated four times, with samples taken every 90 min. After each experiment, the catalyst was cleaned, dried, and then calcined in a muffle furnace at 500 ℃ for 4 h to restore its activity[18]. The SMX removal rate in these four degradation experiments was investigated to analyze the stability of the catalyst.

### 1.4 Analytical Methods

1.4.1 SMX determination

The Ehrlich reaction demonstrates that under acidic conditions, PDAB condenses with sulfonamide groups to form colored Schiff bases, which can absorb UV light and follow the Lambert-Beer law within a specific concentration range. Li *et al*[19] employed spectrophotometry to detect residual sulfonamides in milk and established a linear calibration curve in the range of 3-15 μg/mL. In this study, SMX was quantified via spectrophotometry (with 0.6 mL of PDAB chromogenic reagent added) at a wavelength of 454 nm under the optimized condition of pH=2. The calibration curve was expressed as $y$ = 105.35$x$–0.389 4 ($R^2$=0.999 4) with the range of 1-30 mg/L.

1.4.2 Catalyst characterization

The morphology of the optimal catalyst sample was observed using a SEM at an accelerating voltage of 20 kV. The pore structure and surface functional groups of the catalyst sample were characterized using a FTIR spectrometer over the wavenumber range of 400-4 000 $cm^{-1}$. The XRD patterns of the catalyst were obtained at a tube current of 20 mA, a tube voltage of 40 kV, and a scanning speed of 8 (°/min) over the 2$\theta$ range of 5° to 65°. The XRD patterns of zeolite before and after metal loading were compared with PDF standard cards using Jade 6.5 software to identify the crystalline phases of the catalyst sample.

1.4.3 Copper and manganese quantification

Atomic absorption spectroscopy (AAS)[20] was used to measure the leached concentrations of Cu/Mn and evaluate catalyst stability.

## 2 Results and Discussion

### 2.1 Optimization and Evaluation of Catalyst Preparation Conditions

The results of SMX degradation over the nine prepared catalysts are presented in Table 1, and the results of range analysis for the orthogonal experiment are shown in Table 2. Among the factors affecting catalyst activity and stability, the Cu/Mn molar ratio in the impregnation solution can influence the phase of the catalyst precipitate and induce changes in the structural properties of the catalyst[21]; an excessively high calcination temperature can reduce the specific surface area of the catalyst[22] and alter the morphology of the metal oxide[15]; and an overly long calcination time can damage the pore structure of the support[23]. Tables 1-2 indicate that the optimal combination of the three factors for preparing the most active and stable catalyst is a Cu/Mn molar ratio of 2∶1, a calcination temperature of 300 ℃, and a calcination time of 3 h. Based on the range analysis, the order of factors influencing the SMX removal efficiency was: Calcination temperature (7.59) > Calcination time (3.73) > Cu/Mn molar ratio (2.96). The analysis of variance (ANOVA) (using SPSS 19 software) is shown in Table 3.

By integrating the range analysis from Table 2 and

**Table 1 Original data of SMX removal rate (%) under different catalyst dosage**

| Trial number | Cu/Mn molar ratio | Temperature/℃ | Time/h | Blank column | A/% | B/% | C/% | D/% |
|---|---|---|---|---|---|---|---|---|
| 1-1 | 2∶1 | 300 | 3 | 1 | 77.3 | 68.1 | 75.3 | 73.6 |
| 2-1 | 2∶1 | 400 | 4 | 2 | 57.3 | 54.8 | 71.3 | 61.1 |
| 3-1 | 2∶1 | 500 | 5 | 3 | 73.9 | 69.8 | 65.2 | 69.6 |
| 1-2 | 2∶2 | 300 | 4 | 3 | 63.6 | 74.5 | 63.7 | 67.3 |
| 2-2 | 2∶2 | 400 | 5 | 1 | 60.2 | 63.2 | 65.9 | 63.1 |
| 3-2 | 2∶2 | 500 | 3 | 2 | 69.4 | 66.6 | 65.1 | 67.0 |
| 1-3 | 2∶0.5 | 300 | 5 | 2 | 74.9 | 68.6 | 63.3 | 68.9 |
| 2-3 | 2∶0.5 | 400 | 3 | 3 | 55.7 | 70.2 | 62.4 | 62.8 |
| 3-3 | 2∶0.5 | 500 | 4 | 1 | 64.8 | 66.3 | 60.2 | 63.8 |

A, B, and C represent the SMX removal rates at catalyst dosages of 0.15 g/L, 0.30 g/L, and 0.45 g/L, respectively. D represents the average removal rate of SMX.

**Table 2 Results of range analysis for orthogonal experiment**

%

| Factor | $K_1$ | $K_2$ | $K_3$ | $k^*_1$ | $k^*_2$ | $k^*_3$ | Range |
|---|---|---|---|---|---|---|---|
| Cu/Mn molar ratio | 204.33 | 197.40 | 195.47 | 68.11 | 65.80 | 65.16 | 2.95 |
| Temperatur | 209.77 | 187.00 | 200.43 | 69.92 | 62.33 | 66.81 | 7.59 |
| Time | 203.37 | 192.17 | 201.67 | 67.79 | 64.06 | 67.22 | 3.73 |
| Blank column | 200.43 | 197.10 | 199.67 | 66.81 | 65.70 | 66.56 | 1.11 |

$K_i$, sum of average removal rates corresponding to the *i*-th level of each factor; $k^*_i$, mean value of average removal rates at the *i*-th level of each factor; Range, the difference between the maximum and minimum $k_i$ values for each factor.

**Table 3 Variance analysis of intersubjective effect test**

| Source type | III squared sum | df | Mean square | *F* | Sig. |
|---|---|---|---|---|---|
| Model | 39 753.621[a] | 7 | 5 679.089 | 5 534.035 | 0 |
| Cu/Mn molar ratio | 14.472 | 2 | 7.236 | 7.051 | 0.124 |
| Temperature | 87.341 | 2 | 43.671 | 42.555 | 0.023 |
| Duration | 24.269 | 2 | 12.135 | 11.825 | 0.078 |
| Error | 2.052 | 2 | 1.026 | | |
| Total | 39 755.673 | 9 | | | |

a, predictors(constant); df, degrees of freedom; *F*, *F*-statistic; Sig., significance level (*P*-value).

the significance (Sig.) analysis from Table 3, the influence of the three preparation parameters is ranked as follows: Calcination temperature > Calcination time > Cu/Mn molar ratio in impregnation solution. This observation can be attributed to the dominant role of calcination temperature, which directly affects the morphology of the active metal oxides and the stability of the zeolite support[24]. In contrast, calcination time must be optimized cooperatively with temperature to ensure the complete formation and crystallization of active phases without degrading the support structure. The influence of the Cu/Mn molar ratio becomes more obvious only when suitable calcination conditions are employed, suggesting that it plays a secondary but synergistic role in optimizing catalyst activity.

## 2.2 Catalyst Characterization and Stability

### 2.2.1 SEM analysis

Scanning electron microscopy was used to characterize pristine zeolite and the Cu/Mn-zeolite catalyst. As shown in Fig. 2, the surface of raw zeolite was smooth and uniform. In contrast, the surface of the zeolite after metal loading was relatively rough and layered. It is plausible that the synergetic interaction between copper and manganese promotes the dispersion of metal species on the support, thereby endowing the Cu/Mn catalyst with large pore volume and higher specific surface area[25]. Therefore, the dispersion and adhesion of metal species on the zeolite support generate a better three-dimensional structure, which further increases the specific surface area of the catalyst, raises the number of active sites on its surface, and enhances its catalytic efficiency.

### 2.2.2 FTIR analysis

The FTIR spectrum of the Cu/Mn-zeolite catalyst is shown in Fig. 3. The intense absorption peak near 3 500 $cm^{-1}$ corresponds to the characteristic stretching vibration of surface ·OH and adsorbed water, and the peak at 1 600 $cm^{-1}$ corresponds to the characteristic bending vibration of O-H in crystalline water, indicating that the catalyst possesses excellent hydrophilicity. The hydrophilicity of the catalyst promotes the formation of hydrates and facilitates contact with the reactants. The

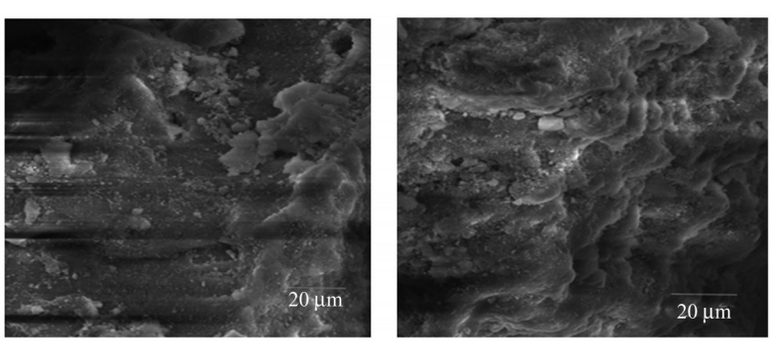


(a) Zeolite (b) Cu/Mn-zeolite catalyst

**Fig. 2 The SEM scanning graph before and after zeolite load**

spectrum shows strong peaks in the range of 1 000-1 100 $cm^{-1}$, which are attributed to the asymmetric stretching absorption peaks of Si-O-Si. This indicates that the catalyst preparation process well preserved the pore structure of the support, which is conducive to the diffusion and adsorption of reactants in the catalyst, thereby improving the catalytic performance. Therefore, the use of zeolite as a support can endow the catalyst with excellent hydrophilicity and porosity, which exerts a positive effect on its catalytic activity[26].

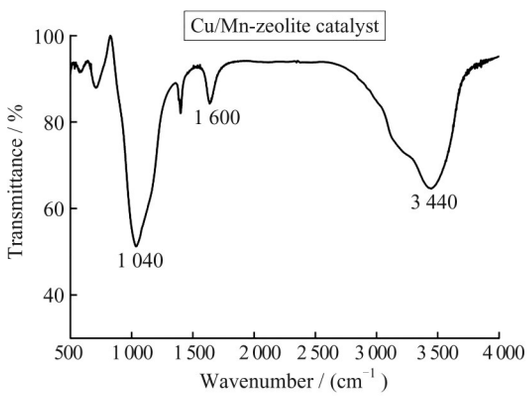


**Fig. 3 FTIR spectrum of the Cu/Mn- zeolite bimetallic catalyst**

2.2.3 XRD analysis

The XRD pattern of the Cu/Mn-zeolite catalyst is presented in Fig. 4. As shown in the figure, the absence of obvious characteristic peaks for the Cu/Mn-zeolite catalyst (along with its weaker diffraction intensity compared with single-metal oxide catalysts) indicates low metal loading, high dispersion, and a less ordered crystal structure[25]. This observation can be attributed to the low metal loading on the zeolite support and the high dispersion of metal crystallites on its surface, both of which lead to a weak diffraction signal[15] . Characteristic peaks corresponding to CuO ($2\theta$=35.597°, 38.757°), $Cu_2O$ ($2\theta$=37.104°), $MnO_2$ ($2\theta$=28.586°, 22.433°, 37.120°), $Mn_3O_4$ ($2\theta$=35.307°, 36.083°, 36.190°), $Cu_2Mn_3O_8$ ($2\theta$=23.218°, 37.120° ), and $CuMn_2O_4$ ($2\theta$ =35.720° , 36.013° ) were identified by comparing the XRD patterns before and after metal loading with PDF standard cards using Jade 6.5 software. These results confirm that Cu and Mn were successfully loaded onto the zeolite surface. These results demonstrate that copper in the Cu/Mn-zeolite catalyst exists mainly as CuO, $Cu_2O$, and Cu/Mn mixed oxides, while manganese exists mainly as $MnO_2$ and $Mn_3O_4$. Notably, the appearance of characteristic peaks for $Cu_2Mn_3O_8$ and $CuMn_2O_4$ confirms that the Cu/Mn-zeolite catalyst forms new crystalline phases (with highly efficient catalytic oxidation properties) via the interaction between copper and mangannese during preparation, rather than being a simple mixture of individual oxides[25]. Moreover, with a higher ratio of surface-adsorbed oxygen to lattice oxygen, $CuMnO_x$ exhibits a greater number of oxygen vacancies than its single-metal counterparts[27]. This defect-rich structure in the as-prepared Cu/Mn-zeolite catalyst enables efficient electron transfer to $H_2O_2$, thereby promoting ·OH generation.

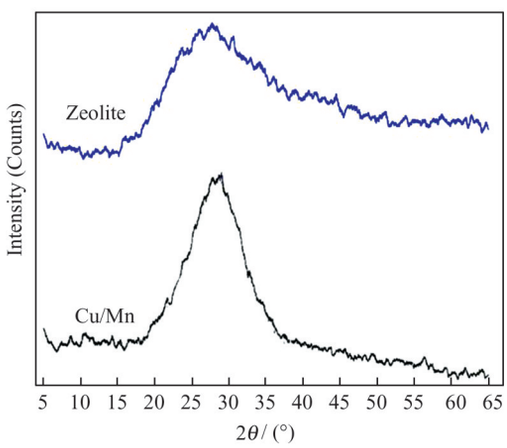


**Fig. 4 XRD patterns of zeolite before and after zeolite loading**

## 2.3 SMX Degradation by UV-Cu/Mn-Zeolite Heterogeneous Fenton

2.3.1 Catalyst dosage effects

Figure 5 presents the effect of varying catalyst dosages on SMX removal efficiency at a fixed $H_2O_2$ concentration of 7.5 mmol/L.

As shown in Fig. 5, the SMX removal efficiency under the three tested catalyst dosages followed the order: 0.15 g/L (highest) > 0.30 g/L > 0.10 g/L(lowest). This can be explained by the fact that the effective metal ion concentration reaches saturation at the optimal catalyst dosage[28], whereas excessive catalyst dosage leads to light saturation. This results in inefficient utilization of photon energy and impairs the direct photolytic degradation by UV irradiation.

2.3.2 $H_2O_2$ dosage effects

Figure 6 shows the effect of $H_2O_2$ dosage on SMX removal efficiency at a fixed catalyst dosage of 0.15 g/L.

Based on Fig. 6, the $H_2O_2$ dosage has a significant impact on the SMX removal rate. When the $H_2O_2$ dosage was 7.5 mmol/L, the SMX removal rate reached the highest value of 77.3%. However, when the $H_2O_2$ dosage

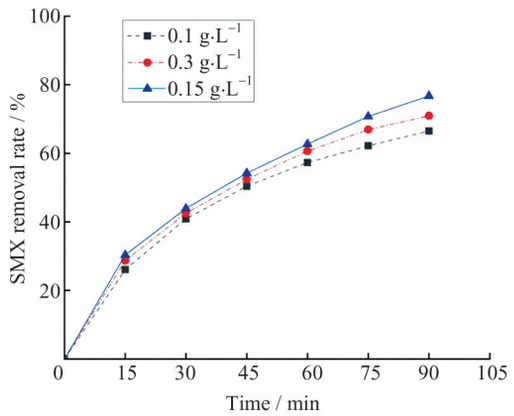


**Fig. 5 Effect of catalyst dosage on SMX degradation efficiency**

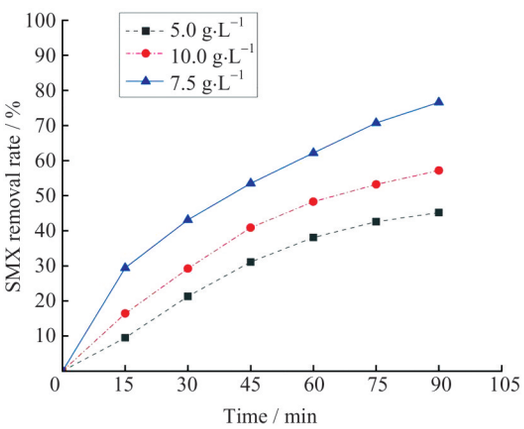


**Fig. 6 Effect of $H_2O_2$ dosage on SMX degradation efficiency**

increased to 10 mmol/L or decreased to 5 mmol/L, the SMX removal rate decreased in both cases. Under the three different dosages, the order of SMX removal rates was as follows: 7.5 mmol/L (highest)>10 mmol/L >5 mmol/L (lowest). This phenomenon can be attributed to the following: when the $H_2O_2$ concentration is relatively low, insufficient ·OH is generated to react with organic pollutants. Conversely, excessive $H_2O_2$ can lead to undesirable side reactions, in which surplus ·OH reacts with $H_2O_2$ to form $HO_2$· (Equation (3)), a radical with weaker oxidizing ability, thereby reducing the oxidation rate of SMX[29].

$$H_2O_2 + \cdot OH \rightarrow \cdot O_2H + H_2O. \quad (3)$$

2.3.3 Comparative studies on the degradation of SMX by UV-$H_2O_2$ oxidation and UV-Cu/Mn-zeolite heterogeneous Fenton oxidation

The SMX removal efficiencies of the UV-$H_2O_2$ oxidation process and the UV-Cu /Mn-zeolite heterogeneous Fenton oxidation process are shown in Fig. 7.

Figure 7 demonstrates that the UV-Cu/Mn-zeolite

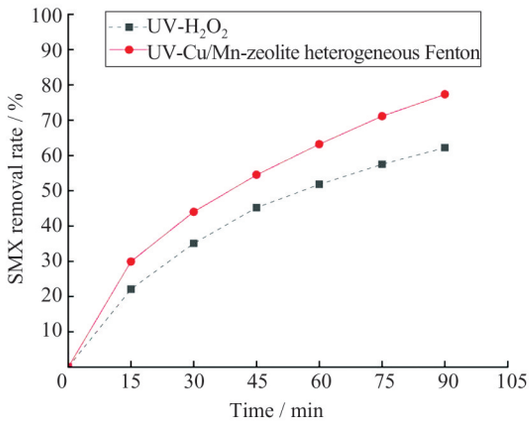


**Fig. 7 SMX removal rate over time for the UV-$H_2O_2$ system and the UV-Cu /Mn-zeolite heterogeneous Fenton system**

heterogeneous Fenton process achieved a 15.1% higher SMX removal efficiency (77.3%) than the conventional UV-$H_2O_2$ process. Previous studies on UV-zeolite-supported monometallic heterogeneous Fenton systems revealed that catalyst adsorption was negligible, contributing less than 3% to SMX removal after 2.5 h of reaction. Therefore, the enhanced SMX removal efficiency observed in this study is mainly attributed to oxidation processes, particularly those involving hydroxyl radicals (·OH) and direct photodegradation. Both the UV-$H_2O_2$ and UV-Cu/Mn-zeolite systems involve the direct photolysis of $H_2O_2$ under UV irradiation to generate hydroxyl radicals, as described in Equation (4). However, in the heterogeneous system, UV irradiation on the catalyst surface also induces the photoexcitation of electrons ($e^-$) and holes ($h^+$), which further promote ·OH production through additional pathways[30]. Furthermore, the synergistic effect between Cu and Mn bimetals optimizes the electron transfer pathway, reduces exciton-hole recombination, and improves the efficiency of ·OH generation[31] (Equations (5) - (7)). In the heterogeneous catalyst system, the transformation of Cu/Mn species promotes the reaction of $H_2O_2$ to generate ·OH for SMX oxidation (Equations (8) and (9))[32].

The combination of direct UV photolysis, exciton-hole generation, and redox cycling of Cu and Mn species significantly enhances the overall generation of hydroxyl radicals, thereby improving SMX degradation. In contrast, UV-mediated direct photodegradation of SMX alone exhibits limited efficiency[29].

$$h\nu + H_2O_2 \rightarrow 2\cdot OH, \quad (4)$$

$$H_2O_2 + e^- \rightarrow \cdot OH + OH^-, \quad (5)$$

$$H_2O + h^+ \rightarrow \cdot OH + H^+, \quad (6)$$

$$OH^- + h^+ \rightarrow \cdot OH, \quad (7)$$

$$Cu^+ + H_2O_2 \rightarrow Cu^{2+} + OH^- + \cdot OH, \quad (8)$$

$$Mn^{2+} + H_2O_2 \rightarrow Mn^{3+} + OH^- + \cdot OH. \quad (9)$$

The experimental data were fitted using the Langmuir-Hinshelwood (L-H) kinetic model. The plots of $\ln(C_0/C)$ versus time, together with the corresponding kinetic parameters for SMX degradation by the UV-$H_2O_2$ process and the UV-Cu/Mn-zeolite heterogeneous Fenton process, are presented in Fig. 8 and Table 3, respectively. As shown, the data for both processes fit the pseudo-first-order kinetic model well, with linear regression coefficients ($R^2$) above 0.98. Furthermore, the SMX degradation rate was faster in the UV/zeolite-supported Cu/Mn bimetallic Fenton system.

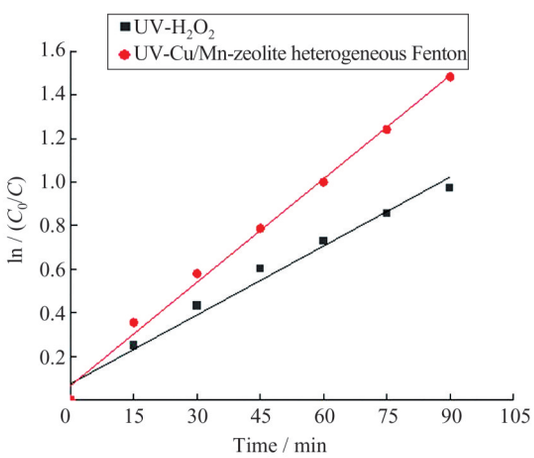


**Fig. 8 Plots of ln($C_0$/$C$) versus time ($t$) for the UV-$H_2O_2$ process and the UV-Cu /Mn-zeolite heterogeneous Fenton process**

UV-mediated direct degradation of SMX exhibits limited efficiency[29], and catalyst adsorption contributes negligibly to SMX removal; thus, hydroxyl radical (·OH) oxidation serves as the main driving mechanism in the UV-Cu/Mn-zeolite heterogeneous Fenton system. The degradation pathways of SMX can be attributed to three possible mechanisms, owing to the susceptibility of its S-N bond, low-bond-energy linkages on the benzene ring, and aromatic structure to attack by hydroxyl radicals (·OH).

1) ·OH-induced cleavage of the S-N bond in SMX generates $C_4H_6N_2O$ (*m*/*z* 98) and $C_6H_6NO_2S$ (*m*/*z* 156). A portion of $C_6H_6NO_2S$ further reacts with ·OH to form $C_6H_7NO_4S$ (*m*/*z* 189)[33-34], as illustrated in Fig. 9.

2) The hydroxyl radical (·OH) attacks the amino group on the benzene ring of SMX, inducing deprotonation to form $C_{10}H_{11}N_3O_4S$ (*m*/*z* 269) [35]. The hydroxylamine group in $C_{10}H_{11}N_3O_4S$ is further oxidized by ·OH to form $C_{10}H_9N_3O_4S$ (*m*/*z* 267) and $C_{10}H_9N_3O_5S$ (m/z 283)[36]. Additionally, ·OH can undergo a substitution reaction with the amino group on the benzene ring of SMX, generating $C_{10}H_{10}N_2O_4S$ (*m*/*z* 254) [37]. Alternatively, ·OH may substitute the methyl group on the isoxazole ring, producing $C_9H_9N_3O_4S$ (*m*/*z* 255)[38]. The proposed degradation pathways are illustrated in Fig. 10.

3)The hydroxyl radical (·OH) can undergo addition reactions with the benzene ring of SMX to form $C_{10}H_{11}N_3O_4S$ (*m*/*z* 270)[33,39], or with the isoxazole ring to produce another isomer of $C_{10}H_{12}N_3O_4S$ (*m*/*z* 270)[40]. The

**Table 3 Kinetic parameters for the degradation of SMX**

| Treatment method | Apparent rate constant/($min^{-1}$) | Initial reaction rate/($mg \cdot L^{-1} \cdot min^{-1}$) | $R^2$ |
|---|---|---|---|
| UV-$H_2O_2$ | 0.010 5 | 0.210 | 0.981 1 |
| UV- Cu /Mn- zeolite heterogeneous Fenton | 0.015 8 | 0.316 | 0.994 3 |

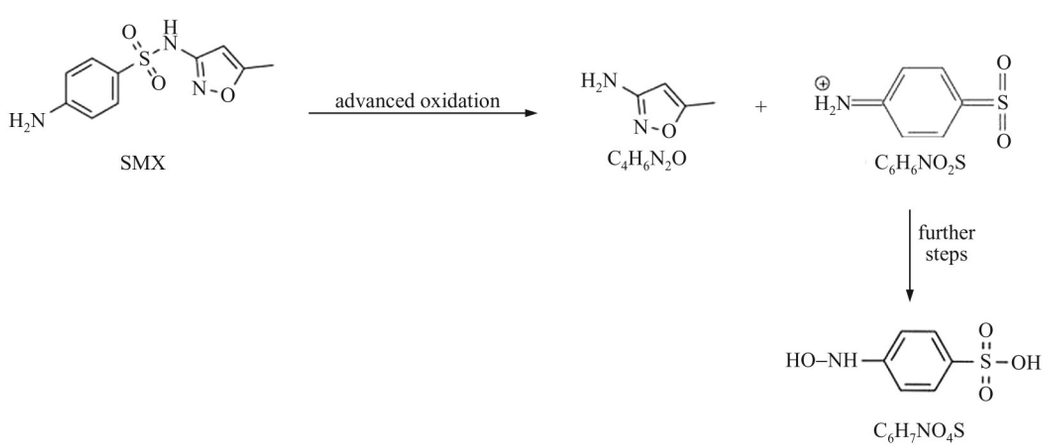


**Fig. 9 Pathway 1 of SMX degradation by advanced oxidation processes**

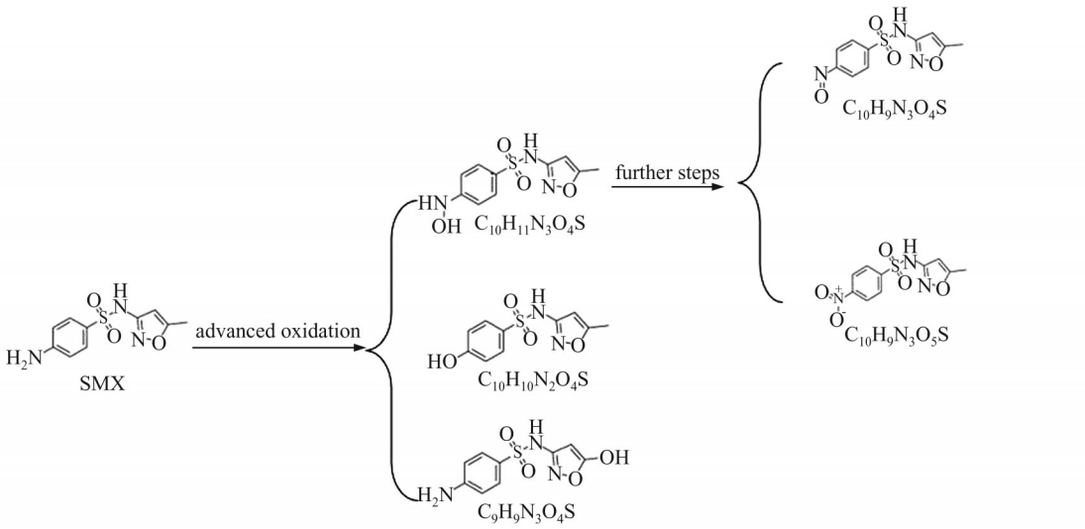


**Fig. 10 Pathway 2 of SMX degradation by advanced oxidation processes**

double bond in the isoxazole ring can be oxidized to form $C_{10}H_{13}N_3O_5S$ (*m*/*z* 287), which subsequently undergoes further oxidation to generate $C_8H_9N_3O_4S$ (*m*/*z* 243), $C_7H_9N_3O_3S$ (*m*/*z* 215), and $C_7H_7N_3O_2S$ (*m*/*z* 197) [33,39]. The proposed degradation pathways are illustrated in Fig. 11.

·OH radicals continue to react with the aforementioned intermediates, partially oxidizing them into simple organic acids such as oxalic acid and acetic acid. These organic acids are subsequently completely mineralized into inorganic compounds[38] (Equations (10)-(11)).

$$C_2H_2O_4 + 2\cdot OH \rightarrow 2H_2O + 2CO_2\,, \qquad (10)$$

$$C_2H_4O_2 + 4\cdot OH \rightarrow 4H_2O + 2CO_2\,. \qquad (11)$$

## 2.4 Catalyst Stability

2.4.1 Metal ion leaching from catalyst

The dynamic leaching profiles of copper and manganese ions in solution are shown in Fig. 12.

As shown in Fig. 12, the leaching concentration for copper remained below 0.3 mg/L throughout the reaction, and that of manganese was consistently below 0.2 mg/L—both significantly lower than the maximum allowable emission limits (0.5 mg/L for total copper and total manganese) stipulated in the "Discharge Standard of Pollutants for Municipal Wastewater Treatment Plants" (GB 18918-2002), demonstrating excellent catalyst stability.

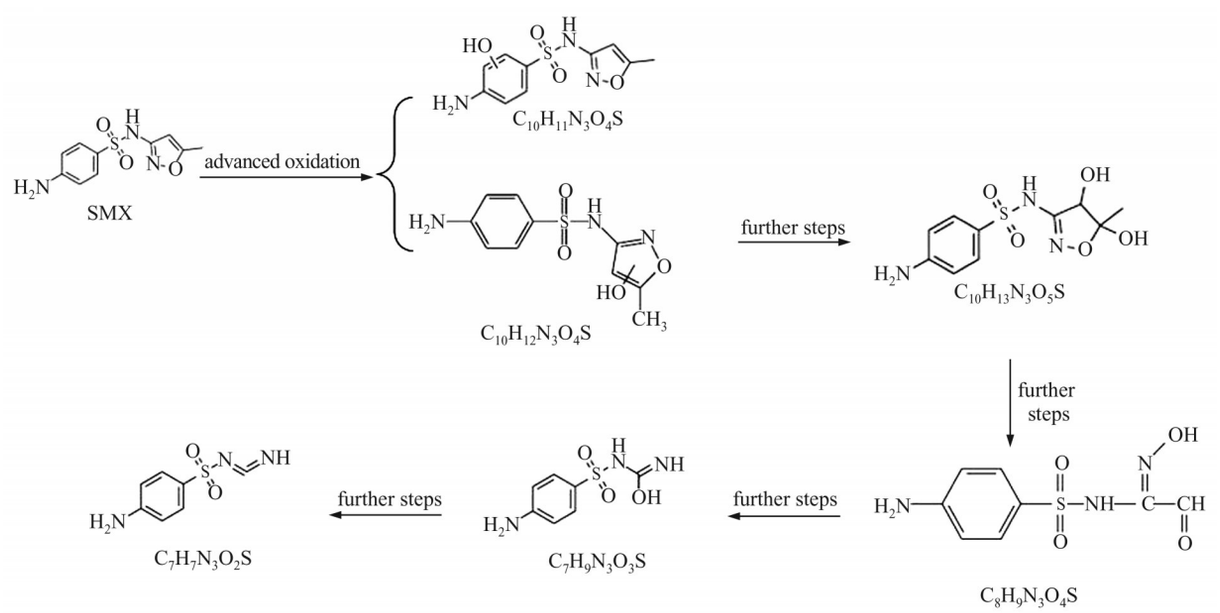


**Fig. 11 Pathway 3 of SMX degradation by advanced oxidation processes**

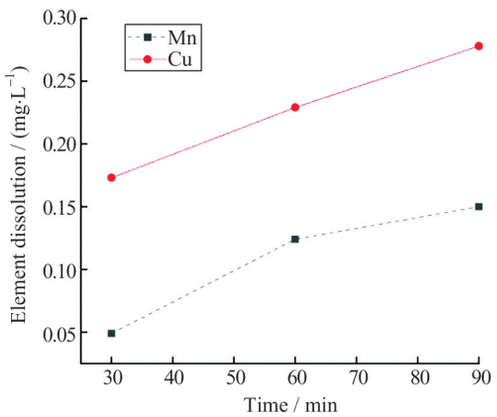


**Fig. 12 Dynamic leaching profiles of Cu and Mn ions from the catalyst during the reaction**

2.4.2 Catalyst reusability

The effect of recycling cycles on SMX degradation efficiency is shown in Fig. 13.

Figure 13 reveals that after four reuse cycles, the SMX removal efficiency of the catalyst decreased from 77.3% to 73.6% within 90 min of reaction, representing a decline of less than 5%. This indicates the high stability of the catalyst prepared under these conditions, which may be attributed to the redox cycling between $Cu^{2+}/Mn^{3+}$ and $H_2O_2$ that generates $Cu^{+}$ and $Mn^{2+}$ to facilitate the regeneration of active sites (Equations (12) and (13)). The standard redox potential of $Cu^{+}/Cu^{2+}$ (0.152 V) is significantly lower than that of $Mn^{2+}/Mn^{3+}$ (1.51V), which thermodynamically favors the oxidation of $Cu^{+}$ to $Cu^{2+}$ by $Mn^{3+}$ [32] (Equation (14)). Concurrently, photogenerated excitons ($e^{-}$) can be captured by $Cu^{2+}$ and $Mn^{3+}$ on the catalyst surface, which are then reduced to $Cu^{+}$ and $Mn^{2+}$ (Equations (15) and (16)), thereby promoting the regeneration of active sites. The slight reduction in catalytic efficiency after repeated cycles may result from the partial blockage of active sites by pollutants or leached metal ions [41].

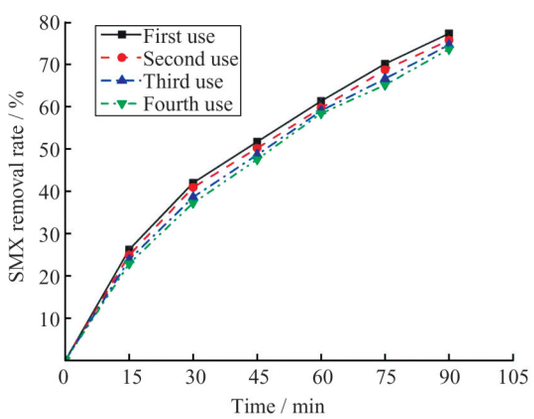


**Fig. 13 Effect of recycling cycles on the catalytic performance of the catalyst at different reaction time**

$$Cu^{2+} + H_2O_2 \rightarrow Cu^{+} + \cdot O_2H + H^{+}, \quad (12)$$

$$Mn^{3+} + H_2O_2 \rightarrow Mn^{2+} + \cdot O_2H + H^{+}, \quad (13)$$

$$Cu^{+} + M_n{}^{3+} \rightarrow Cu^{2+} + Mn^{2+}, \quad (14)$$

$$Cu^{2+} + e^{-} \rightarrow Cu^{+}, \quad (15)$$

$$Mn^{3+} + e^{-} \rightarrow Mn^{2+}. \quad (16)$$

## 3 Conclusion

The Cu/Mn-zeolite catalyst, prepared with a Cu/Mn molar ratio of 2∶1 in the impregnation solution and calcined at 300 ℃ for 3 h, exhibits an excellent three-dimensional porous structure, outstanding hydrophilicity, and high catalytic activity.

Structural characterization confirms that the metal components in the catalyst exist mainly in crystalline phases. Copper is predominantly present as CuO, $Cu_2O$, and Cu/Mn oxides, while manganese mainly exists as $MnO_2$ and $Mn_3O_4$. Notably, new crystalline phases are formed during catalyst preparation due to the interaction between the two metals, which further enhances the redox properties of the catalyst.

Under near-neutral pH conditions with an initial SMX concentration of 20 mg/L, a catalyst dosage of 0.15 g/L, and an $H_2O_2$ dosage of 7.5 mmol/L, the UV-Cu/Mn-zeolite heterogeneous Fenton process achieved an SMX removal efficiency of 77.3%, representing a 15.1% improvement compared with the UV-$H_2O_2$ process. The degradation followed pseudo-first-order kinetics. The metal leaching concentrations remained below 0.5 mg/L, and the catalyst exhibited satisfactory stability with less than a 5% activity loss after four reuse cycles.

## References

[1] Cui H, Tian Y, Zhang J. Degradation of sulfonamide antibiotics by intermittent ultrasound enhanced ZVI/PS process[J]. *Research of Environmental Sciences*, 2021, **34**(12): 2820-2830(Ch).

[2] Song Y L, Qi J Y, Tian J Y, *et al*. Construction of Ag/g-$C_3N_4$ photocatalysts with visible-light photocatalytic activity for sulfamethoxazole degradation[J]. *Chemical Engineering Journal*, 2018, **341**: 547-555.

[3] En L E, Sahu R S, Chen W L, *et al*. Effective photocatalytic degradation of sulfamethoxazole using tunable $CaCu_3Ti_4O_7$

perovskite[J]. *Chemosphere*, 2022, **294**: 133744.

[4] Miran W, Jang J, Nawaz M, *et al*. Biodegradation of the sulfonamide antibiotic sulfamethoxazole by sulfamethoxazole acclimatized cultures in microbial fuel cells[J]. *Science of the Total Environment*, 2018, **627**: 1058-1065.

[5] Chi X, Zhou W B, Wu L, *et al*. Removal of three kinds of tetracycline antibiotics and three kinds of sulfa antibiotics in biogas slurry by Fenton oxidation[J]. *Journal of Agro-Environment Science*, 2018, **37**(11): 2451-2455(Ch).

[6] Zhao S X, Liu L H, Zhang X H, *et al*. Study on oxidative degradation of sulfamethoxazole in water by Fenton method [J]. *Technology of Water Treatment*, 2022, **48**(8): 63-66(Ch).

[7] Li H L, Cheng F, Shi D N, *et al*. Catalytic mechanism and strategies for enhancing performance of heterogeneous Fenton catalysts: A review[J]. *Industrial Water Treatment*, 2023, **43**(11): 78-92(Ch).

[8] Zhang M H, Dong H, Zhao L, *et al*. A review on Fenton process for organic wastewater treatment based on optimization perspective[J]. *Science of the Total Environment*, 2019, **670**: 110-121.

[9] Wang K Y, Ding J Q, Li Z Y, *et al*. Degradation of norfloxacin by Fenton-like and photo-Fenton processes catalyzed by $BiFeO_3$[J]. *China Water & Wastewater*, 2019, **35**(9): 48-52 (Ch).

[10] Kim E J, Oh D, Lee C S, *et al*. Manganese oxide nanorods as a robust Fenton-like catalyst at neutral pH: Crystal phase-dependent behavior[J]. *Catalysis Today*, 2017, **282**: 71-76.

[11] Jiang S L, Tang Y, Li C H, *et al*. Novel bimetallic A-$MnO_x$ catalysts for the photothermal catalytic degradation of toluene[J]. *Journal of Guangxi University* (*Natural Science Edition*), 2022, **47**(6): 1651-1661(Ch).

[12] Zhao W J, Zhang J R, Du X R, *et al*. Research progress of low temperature deoxidation catalysts for syngas[J]. *Petrochemical Industry Technology*, 2025, **32**(1): 4-6, 124. (Ch)

[13] Fu J W, Chen S S, Fang K L, *et al*. Advantage of microreactor on the synthesis of high-activity Cu-Mn catalyst by co-precipitation[J]. *CIESC Journal*, 2023, **74**(2): 776-783(Ch).

[14] Duan Y X, Liu P X, Lin F W, *et al*. Catalytic ozonation of dichloromethane at low temperature and even room temperature on Mn-loaded catalysts[J]. *RSC Advances*, 2022, **12** (51): 33429-33439.

[15] Wang H P, Lu Y Y, Han Y X, *et al*. Enhanced catalytic toluene oxidation by interaction between copper oxide and manganese oxide in Cu-O-Mn/γ-$Al_2O_3$ catalysts[J]. *Applied Surface Science*, 2017, **420**: 260-266.

[16] Zhang L, Perales-Rondón J V, Thomère A, *et al*. Platinum-zeolite hybrid catalyst for the electrooxidation of formic acid [J]. *Journal of Electroanalytical Chemistry*, 2021, **896**: 115491.

[17] Tang H L. The *Treatment of Sulfamethoxazole Wastewaterby UV-$H_2O_2$ and UV-Heterogeneous Fenton*[D]. Chongqing: Chongqing University, 2018(Ch).

[18] Martínez T L M, Muñoz A, Pérez A, *et al*. The effect of support surface hydroxyls on selective CO methanation with Ru based catalysts[J]. *Applied Catalysis A*: *General*, 2022, **641**: 118678.

[19] Li X B, Hou Y Z, Li J J. Determination of sulfonamide residues in milk by spectrophotometry[J]. *China Dairy*, **2008** (11): 54-56(Ch).

[20] Yang Y H, Feng P, Bian L N, *et al*. The Principle, advantages and applications of atomic absorption spectroscopy in detecting heavy metals in food[J]. *The Food Industry*, **2024**(23): 119-121(Ch).

[21] Hu Y H, Zuo S X, Yao C. Hydrothermal preparation of Cu-Mn catalyst and its catalytic performance[J]. *Chemical Engineering Journal*, 2023, **51**(8): 18-22(Ch).

[22] Konsolakis M, Stathopoulos V N. Rational design of non-precious metal oxide catalysts by means of advanced synthetic and promotional routes[J]. *Catalysts*, 2021, **11**(8): 895.

[23] Ogura Y, Asai T, Sato K, *et al*. Effect of calcination and reduction temperatures on the catalytic activity of Ru/$La_{0.5}Ce_{0.5}O_{1.75}$ for ammonia synthesis under mild conditions [J]. *Energy Technology*, 2020, **8**(6): 2000264.

[24] Li J Q, Liu M X, Chu Q R, *et al*. Effects of calcination temperature on catalytic performance of Ru/$CeO_2$ catalysts for hydrogen production by high flux steam reforming of methanol[J]. *Low-Carbon Chemistry and Chemical Engineering*, 2025, **50**(3): 23-29(Ch).

[25] Xu Z Z, Tang J, Wang R, *et al*. Selective catalytic oxidation of N,N-dimethylacetamide on composite catalyst of Cu-Mn metallic oxide and $Cu^{2+}$-exchanged ZSM-5 zeolite[J]. *Environmental Chemistry*, 2025, **44**(9): 3415-3425(Ch).

[26] Wang B, Yang Y H, Yang Y X. Heterogeneous Fenton oxidation performance of vanadium-doped copper-based and iron-based bimetallic catalysts[J]. *Chemical Industry and Engineering Progress*, 2021, **40**(12): 6705-6713(Ch).

[27] Yang X N, Luo L N, Zhou J Y, *et al*. Catalytic combustion performance of copper manganese catalyst for lowconcentration ethanol[J]. *Journal of Environmental Engineering Technology*, 2023, **13**(2): 527-533(Ch).

[28] Song H Y, You J G, Chen C X, *et al*. Manganese functionalized mesoporous molecular sieves Ti-HMS as a Fenton-like catalyst for dyes wastewater purification by advanced oxidation processes[J]. *Journal of Environmental Chemical Engineering*, 2016, **4**(4): 4653-4660.

[29] Zhu H Q, Liu C, Wang B, *et al*. Performance of oxidation

and degradation of trace sulfamethoxazole (SMX) with UV/immobilized $TiO_2$[J]. *Water Purification Technology*, 2014, **33**(1): 83-87(Ch).

[30] Liu H, Wu N N. Research progress on photocatalytic degradation of antibiotics and reuse of catalysts[J]. *Modern Chemical Industry*, 2024, **44**(3): 58-61, 68(Ch).

[31] Chen N L, Wei D M, Meng Y F, *et al*. Researches status of heterogeneous photo Fenton catalysts[J]. *Applied Chemical Industry*, 2021, **50**(8): 2269-2274, 2279(Ch).

[32] Su Y P, Long Y K, Chen J J, *et al*. *In situ* synthesis of tree-branch-like copper-manganese oxides nanoarrays supported on copper foam as a superior efficiency Fenton-like catalyst for enhanced degradation of 4-chlorophenol[J]. *Applied Surface Science*, 2022, **593**: 153241.

[33] Liu G F, Li X C, Han B J, *et al*. Efficient degradation of sulfamethoxazole by the Fe(II)/$HSO_5^-$ process enhanced by hydroxylamine: Efficiency and mechanism[J]. *Journal of Hazardous Materials*, 2017, **322**: 461-468.

[34] Zhu L, Shen Y, Gong Y H, *et al*. Bio-synthesis of manganese oxides and its efficient activation of periodate for sulfamethoxazole degradation[J]. *Journal of Anhui Agricultural University*, 2025, **52**(4): 701-708(Ch).

[35] Pan X Y, Sun Y D, Xia L G, *et al*. Synergistic effect of *in situ* generated hydrogen peroxide on the degradation of sulfamethoxazole (SMX) by 1T-2H phase $MoS_2$-activated PAA [J]. *Separation and Purification Technology*, 2025, **359**: 130573.

[36] Kong D W, Xu Q, Wang Y X, *et al*. Degradation of sulfamethoxazole *via* electrochemical and Fe(III)-enhanced activation of sodium bisulfite[J]. *Modern Chemical Research*, **2025**(5): 188-190(Ch).

[37] Wang G S, Fu D B, Liu Y Q, *et al*. Photochemical degradation of sulfamethoxazole by UV/$NO_3^-$ in water[J]. *Acta Scientiae Circumstantiae*, 2020, **40**(4): 1234-1241(Ch).

[38] Wang A M, Li Y Y, Estrada A L. Mineralization of antibiotic sulfamethoxazole by photoelectro-Fenton treatment using activated carbon fiber cathode and under UVA irradiation[J]. *Applied Catalysis B*: *Environmental*, 2011, **102**(3/4): 378-386.

[39] Han X, Zhou C L, Chen Y J, *et al*. Preparation of Yb-Sb Co-doped Ti/SnO(2) electrode for electrocatalytic degradation of sulfamethoxazole (SMX) [J]. *Chemosphere*, 2023, **339**: 139633.

[40] Zhao S X, Liu L H, Zhang X H, *et al*. Study on oxidative degradation of sulfamethoxazole in water by Fenton method [J]. *Technology of Water Treatment*, 2022, **48**(8): 63-66(Ch).

[41] Gao Z X, Yang W L . Preparation of the catalyst for antibiotic wastewater treatment by catalytic ozonation[J]. *Technology of Water Treatment*, 2018, **44**(3): 39-44(Ch).

# UV-沸石负载Cu/Mn双金属非均相Fenton法降解磺胺甲恶唑

秦涛[1]， 汤红亮[1]， 郑良秋[1]， 丁思铖[2]， 李建兵[3]， 曾晓岚[1†]

1.重庆大学 环境与生态学院，重庆 400045

2.美国杜克大学 化学系，北卡罗来纳 达勒姆 27708

3.加拿大北英属哥伦比亚大学 工程学院，不列颠哥伦比亚省 乔治王子城 V2N4Z9

**摘要：**磺胺甲恶唑（Sulfamethoxazole，SMX）等抗生素在低浓度下即可对人类和环境产生危害，单纯采用物化、生化技术降解效果不佳。本文采用光催化与非均相Fenton技术结合的方式对SMX进行处理，并比较了UV-$H_2O_2$和UV-沸石负载Cu/Mn双金属非均相Fenton法对SMX的去除效果。结果表明，焙烧温度、焙烧时长、浸渍液Cu/Mn摩尔比对催化剂活性的影响程度依次降低。在Cu/Mn摩尔比2∶1，焙烧温度300 ℃，焙烧时长3 h条件下制备的催化剂性能最佳。催化剂中Cu和Mn分别主要以CuO、$Cu_2O$、Cu/Mn氧化物和$MnO_2$、$Mn_3O_4$等形式存在。在pH=7.2、初始SMX浓度为20 mg/L，催化剂最优投加量为0.15 g/L，$H_2O_2$最优投加量为7.5 mmol/L时，UV-沸石负载Cu/Mn双金属非均相Fenton法对SMX的去除率为77.3%，相比UV-$H_2O_2$法增加了15.1%，其降解过程符合一级反应动力学方程。反应90 min催化剂的金属析出量均低于0.5 mg/L，经过四次重复利用，其活性下降不到5%，具有良好的稳定性。

**关键词：**Cu/Mn-沸石催化剂；UV-非均相Fenton体系；磺胺甲恶唑；最优制备条件；反应条件；催化剂稳定性

□